

# Comparative efficiency analysis of GaN-based light-emitting diodes and laser diodes

Joachim Piprek<sup>a)</sup>

NUSOD Institute LLC, Newark, Delaware 19714-7204, USA

(Received 23 May 2016; accepted 29 June 2016; published online 11 July 2016)

Nobel laureate Shuji Nakamura predicted in 2014 that GaN-based laser diodes are the future of solid state lighting. However, blue GaN-lasers still exhibit less than 40% wall-plug efficiency, while some GaN-based blue light-emitting diodes exceed 80%. This paper investigates non-thermal reasons behind this difference. The inherently poor hole conductivity of the Mg-doped waveguide cladding layer of laser diodes is identified as main reason for their low electrical-to-optical energy conversion efficiency. *Published by AIP Publishing.* [<http://dx.doi.org/10.1063/1.4958619>]

Shuji Nakamura predicted in his Nobel lecture that GaN-based laser diodes (LDs) may enable the next generation of solid state lighting,<sup>1</sup> which is mainly driven by the promise of high electrical-to-optical energy conversion efficiency, also referred to as wall-plug efficiency  $\eta_{\text{WPE}}$ . GaN-based blue light-emitting diodes (LEDs) achieve up to  $\eta_{\text{WPE}} = 84\%$ ,<sup>2</sup> but the highest  $\eta_{\text{WPE}}$  values reported for GaN-based laser diodes (LDs) are still below 40%.<sup>3–5</sup> This paper analyzes the reasons for this  $\eta_{\text{WPE}}$  difference by comparative numerical simulation of both device types based on the same active region design and the same material properties. Simulation results are validated by LED and LD measurements.

The wall-plug efficiency  $\eta_{\text{WPE}}$  is defined as ratio of light output power to electrical input power  $IV$  ( $I$ -current,  $V$ -bias). It is connected to the external quantum efficiency  $\eta_{\text{EQE}} = \eta_{\text{WPE}}/\eta_{\text{ELE}}$  by the electrical efficiency  $\eta_{\text{ELE}} = h\nu/qV$  ( $h\nu$ -photon energy,  $q$ -electron charge). The external quantum efficiency  $\eta_{\text{EQE}}$  is the ratio of emitted photon number to injected number of electron-hole pairs. The conversion of electron-hole pairs into emitted photons is accompanied by carrier losses and by photon losses, which are described by the internal quantum efficiency  $\eta_{\text{IQE}}$  and the photon extraction efficiency  $\eta_{\text{EXE}}$ , respectively, in the case of LEDs ( $\eta_{\text{EQE}} = \eta_{\text{IQE}} \eta_{\text{EXE}}$ ).<sup>6</sup> With LDs,  $\eta_{\text{EQE}}$  is typically split up into the slope efficiency  $\eta_{\text{S}}$  and the threshold efficiency  $\eta_{\text{th}} = (I - I_{\text{th}})/I$  ( $I_{\text{th}}$ —threshold current,  $\eta_{\text{EQE}} = \eta_{\text{th}} \eta_{\text{S}}$ ).<sup>7</sup> Our comparison focuses on  $\eta_{\text{EQE}}$  and  $\eta_{\text{WPE}}$  which are defined the same way for LEDs and LDs.

We employ advanced device simulation software<sup>8</sup> which self-consistently computes carrier transport, the wurtzite electron band structure of strained InGaN quantum wells (QWs), and photon emission. Schrödinger and Poisson equations are solved iteratively in order to account for the QW deformation with changing device bias (quantum-confined Stark effect). The transport model includes drift and diffusion of electrons and holes, Fermi statistics, built-in polarization and thermionic emission at hetero-interfaces, as well as all relevant radiative and non-radiative recombination mechanisms. For clarity, self-heating is excluded in this study, and all results are reported

for room temperature ( $T = 300$  K). More details on the employed device models are given elsewhere.<sup>9</sup>

Our study starts with a calibration and validation of the device model by simulating the measured performance of a blue LED that comprises a single 3 nm thick InGaN QW and a 20 nm thick Mg-doped AlGaIn electron blocking layer (EBL).<sup>10,11</sup> The energy band diagram in Fig. 1 shows the strong QW deformation by the built-in polarization field which separates electrons and holes. Key material parameters are obtained by simultaneously fitting measurements of light output power, bias, and emission wavelength (Fig. 2). The latter was reproduced by using a QW material band gap of 2.848 eV and a common conduction band offset ratio of 0.7. The QW polarization was extracted from reproducing the blue-shift of the photon energy due to screening by the rising QW carrier density. The resulting QW interface charge density of  $1.3 \times 10^{13} \text{ cm}^{-2}$  is about 80% of the value predicted by Bernardini<sup>12</sup> and about 70% of the value predicted by Pal *et al.*<sup>13</sup> Carrier leakage from the QW is found to be negligibly small so that the quantum efficiency droop in Fig. 2 is solely caused by QW Auger recombination. Our  $\eta_{\text{IQE}}$  fit is based on a Shockley-Read-Hall recombination lifetime of 45 ns and an

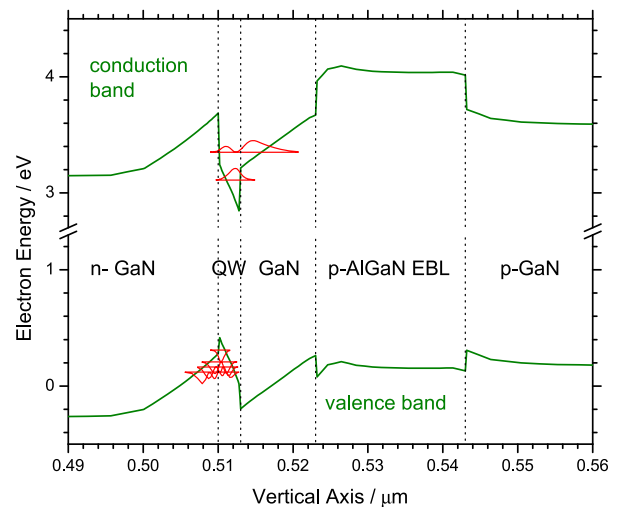


FIG. 1. Energy band diagram (green) and InGaIn quantum well (QW) energy levels with wave functions (red) as calculated for the reference LED structure at  $100 \text{ A/cm}^2$  current density.

<sup>a)</sup>E-mail: piprek@nusod.org

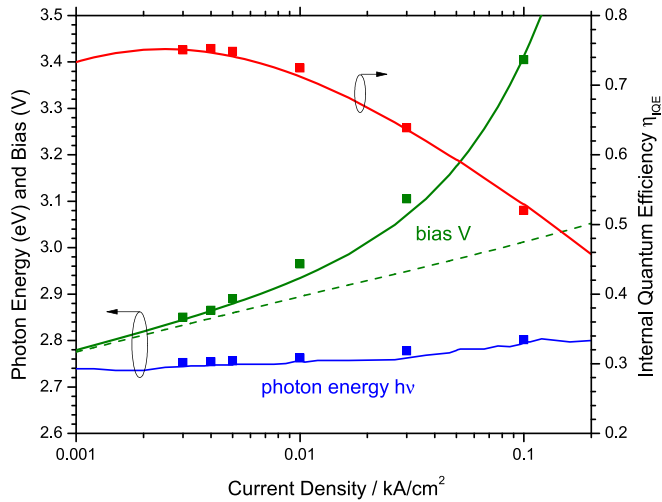


FIG. 2. Comparison between LED measurements (symbols)<sup>11</sup> and simulations (lines). The dashed line gives the bias without contact resistance. The LED chip size is  $200 \mu\text{m} \times 200 \mu\text{m}$ .

Auger recombination coefficient of  $C = 7 \times 10^{-31} \text{ cm}^6/\text{s}$ , which is close to literature data.<sup>14</sup> The photon generation rate is calculated self-consistently without using the common fit parameter B. The bias-current characteristic in Fig. 2 reveals a relatively high contact resistance that is not typical for industry-grade devices and is therefore neglected in the following. The remaining series resistance is about  $0.1 \Omega$  and it is dominated by the low hole conductivity. The Mg acceptor ionization energy scales linearly between 170 meV for GaN and 470 meV for AlN and it keeps the density of free holes low, despite the high acceptor density of  $10^{19} \text{ cm}^{-3}$ . The assumed hole mobility is  $10 \text{ cm}^2/\text{Vs}$  and it gives a p-GaN resistivity of  $1.5 \Omega\text{cm}$  in good agreement with measurements.<sup>15</sup> A more detailed discussion of GaN-LED modeling issues can be found elsewhere.<sup>16</sup>

For laser simulation, we embed the LED layers from Fig. 1 into a GaN waveguide that is sandwiched between AlGaIn cladding layers. Vertical profiles of refractive index and guided laser mode are shown in Fig. 3. The optical

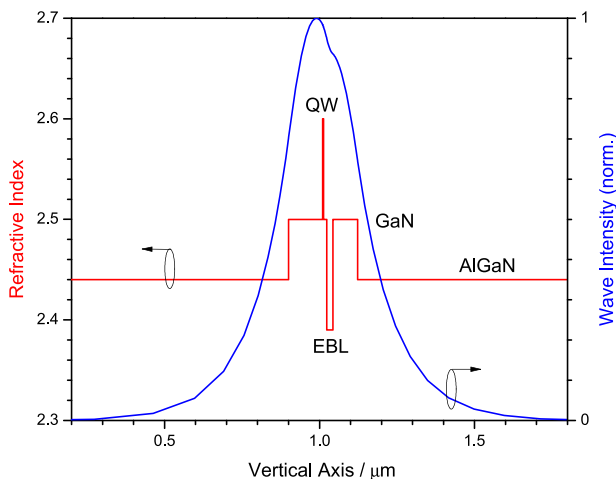


FIG. 3. Vertical profiles of refractive index and wave intensity for the laser diode using the same InGaIn quantum well (QW) and AlGaIn electron blocking layer (EBL) as in the LED (see Fig. 1).

confinement factor is  $\Gamma = 0.76\%$ . Our broad-area Fabry-Perot laser is  $50 \mu\text{m}$  wide and  $800 \mu\text{m}$  long so that the active area is the same as with the LED. The facet reflectance is 0.05 and 0.95, respectively.<sup>5</sup> However, the additional p-AlGaIn cladding layer raises the series resistance to about  $0.5 \Omega$ , despite our quite optimistic assumption of  $10 \text{ cm}^2/\text{Vs}$  hole mobility. Practical AlGaIn mobility values may be substantially lower. The Mg acceptor density is kept at  $10^{19} \text{ cm}^{-3}$  resulting in a p-AlGaIn cladding layer resistivity of about  $2 \Omega\text{cm}$ , which is close to literature data.<sup>15</sup>

The simulated external quantum efficiencies are compared in Fig. 4. Similar and relatively low optical losses are assumed in both cases with  $\eta_{\text{EXE}} = 80\%$  for the LED and  $\alpha_i = 5/\text{cm}$  for the LD, translating into  $\eta_S = 79\%$  (solid lines). Without optical loss,  $\eta_{\text{EQE}}$  is enhanced significantly and the dashed LED line is identical to  $\eta_{\text{IQE}}$  in Fig. 2. The laser slope efficiency is  $\eta_S = 100\%$  in this case, due to the absence of carrier leakage. If Auger recombination is also eliminated from the simulation, the LED quantum efficiency approaches unity without any efficiency droop, and the laser threshold current density is reduced to less than  $300 \text{ A/cm}^2$  ( $C = 0$ , dashed-dotted lines). In all these cases, the maximum LD efficiency at high current surpasses the peak LED efficiency at low current, as anticipated by Nakamura (cf. Fig. 17 in Ref. 1). The key reason for this laser advantage is the clamping of the QW carrier population at the lasing threshold density, so that carrier losses do not increase any further with rising current and any additional electron hole-pair turns into a photon. Thus,  $\eta_{\text{EQE}} = \eta_{\text{th}} \eta_S$  keeps rising with higher current in Fig. 4 and saturates at the slope efficiency  $\eta_S$ . However, we neglect self-heating here, which would lead to increasing QW carrier density and therefore to increasing carrier losses above lasing threshold.<sup>17</sup>

The simulated wall-plug efficiency produces a much different picture (Fig. 5). The peak LD efficiency is now significantly lower than the maximum LED efficiency, but it occurs at much higher output power (see inset of Fig. 5). The

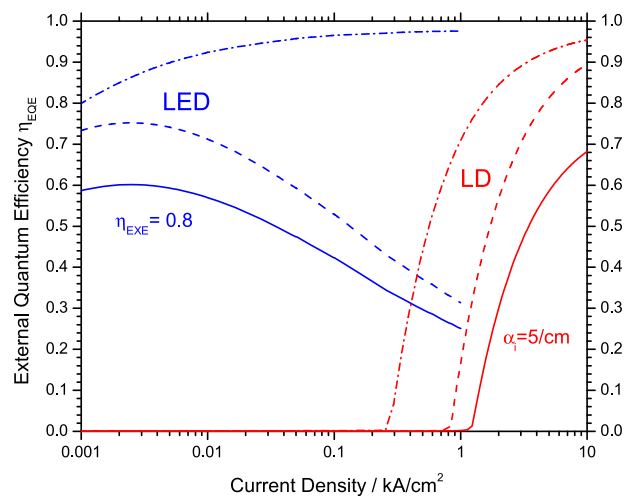


FIG. 4. Comparison of the simulated external quantum efficiency  $\eta_{\text{EQE}}$  vs. current density for the reference LED (blue) and the laser diode (red). (solid: comparable optical loss; dashed: no optical loss; dashed-dotted: no optical loss and no Auger recombination).

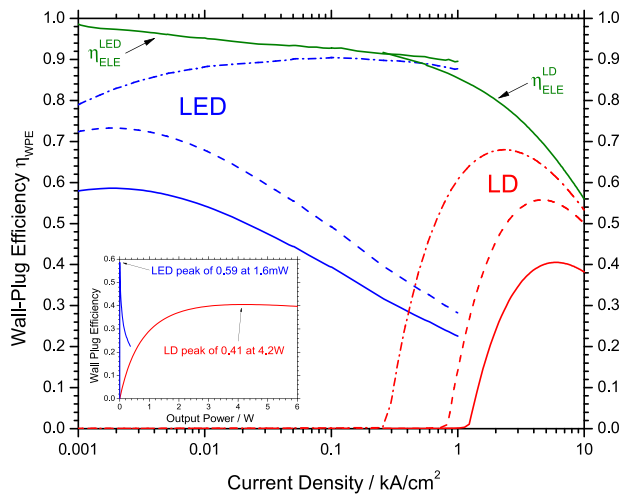


FIG. 5. Comparison of the simulated wall-plug efficiency  $\eta_{\text{WPE}}$  vs. current density for the reference LED (blue) and the laser diode (red). (Solid: comparable optical loss; dashed: no optical loss; dashed-dotted: no optical loss and no Auger recombination.) The green lines show the electrical efficiency  $\eta_{\text{ELE}}$  for LED and LD, respectively. The inset plots the wall plug efficiency with optical loss vs. output power for both device types.

predicted laser characteristic (red solid line) is quite close to recent laser measurements.<sup>5</sup> The LED wall-plug efficiency is clearly limited by QW Auger recombination, which also contributes to the high lasing threshold. But even without Auger recombination, both devices now exhibit efficiency droop with higher currents. The reason is the strong decline of the electrical efficiency  $\eta_{\text{ELE}}$  with higher current density (green lines in Fig. 5). Since laser diodes operate at higher current than LEDs, their bias is higher and their peak  $\eta_{\text{WPE}}$  is lower, even under idealized circumstances. This natural difference is dramatically enhanced by the low hole conductivity of Mg-doped layers and the resulting series resistance. Lasers require thicker p-cladding layers for waveguiding and therefore exhibit an even higher bias. Higher Mg doping is not a viable solution because of acceptor density saturation and because heavy Mg doping reduces the hole mobility by enhanced scattering. It also contributes to photon absorption.<sup>18</sup> Therefore, alternative solutions are currently explored, such as undoped waveguide layers,<sup>5</sup> tunnel junction contacts,<sup>19</sup> and indium-tin-oxide cladding layers.<sup>15</sup>

Our somewhat idealized comparison overestimates the efficiency by neglecting the effects of self-heating, lateral carrier spreading, and possible vertical carrier leakage. For comparison and validation, we therefore extend this study by a simple analysis of recently published continuous-wave measurements on 405 nm laser diodes showing a record-high 7.2 W output power at  $I = 4$  A and  $V = 6.3$  V at room temperature.<sup>5</sup> These lasers exhibit a low thermal resistance ( $R_{\text{th}} = 6$  K/W)<sup>20</sup> and an optimized waveguide structure with low optical loss ( $\alpha_i = 2/\text{cm}$ ). Utilizing the method published by Crump *et al.*,<sup>7</sup> we extract the following efficiency data directly from the measured light power and bias characteristics as given in Fig. 13(b) of Ref. 5. The results are plotted in Fig. 6. The laser wall-plug efficiency is split into the electrical efficiency  $\eta_{\text{ELE}}$ , the threshold efficiency  $\eta_{\text{th}}$ , and the slope efficiency  $\eta_{\text{S}}$ . The electrical efficiency dominates at high current, in

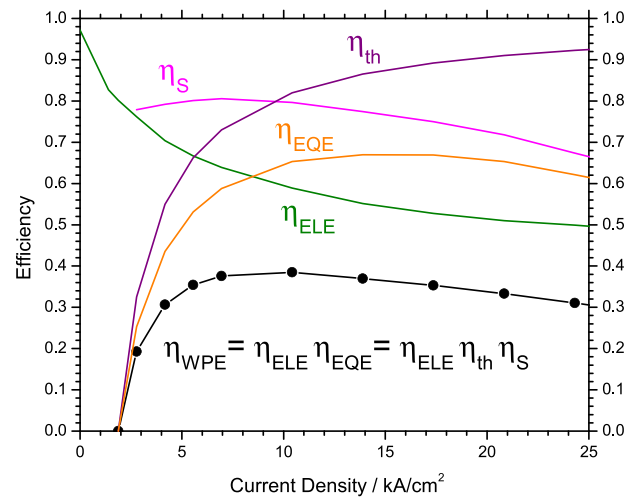


FIG. 6. Efficiencies extracted from recently published measurements on 405 nm GaN-based laser diodes.<sup>5</sup>

excellent agreement with our analysis in Fig. 5. The slope efficiency also decreases due to thermally enhanced loss mechanisms such as Auger recombination or electron leakage. The threshold efficiency  $\eta_{\text{th}} = (I - I_{\text{th}})/I$  approaches unity at high current, i.e., QW Auger recombination has less influence on the high-power wall-plug efficiency than the series resistance, as predicted above. The peak external quantum efficiency is  $\eta_{\text{EQE}} = 67\%$  for this laser, which is close to typical GaN-LED results.

In conclusion, the external quantum efficiency of GaN lasers can be expected to exceed that of GaN LEDs, but the record wall-plug efficiency of 84% reported for GaN-LEDs seem out of reach for GaN-lasers, mainly due to the higher bias which is the natural consequence of the much higher current and the inherently low hole conductivity of Mg-doped layers. However, laser diodes exhibit a clear efficiency advantage over LEDs at higher output power.

<sup>1</sup>S. Nakamura, *Ann. Phys.* **527**, 335 (2015).

<sup>2</sup>C. A. Humi, A. David, M. J. Cich, R. I. Aldaz, B. Ellis, K. Huang, A. Tyagi, R. A. DeLille, M. D. Craven, F. M. Steranka, and M. R. Krames, *Appl. Phys. Lett.* **106**, 031101 (2015).

<sup>3</sup>J. W. Raring, in DOE SSL R&D Workshop, Raleigh, 2016.

<sup>4</sup>A. Loeffler, C. Eichler, J. Mueller, S. Gerhard, B. Stojetz, S. Tautz, C. Vierheilg, J. Ristic, A. Avramescu, M. Horn, T. Hager, C. Walter, T. Dobbertin, H. Koenig, and U. Strauss, *Proc. SPIE* **9363**, 936318 (2015).

<sup>5</sup>M. Kawaguchi, O. Imafuji, S. Nozaki, H. Hagino, S. Takigawa, T. Katayama, and T. Tanaka, *Proc. SPIE* **9748**, 974818 (2016).

<sup>6</sup>J. Piprek, *Phys. Status Solidi A* **207**, 2217 (2010).

<sup>7</sup>P. Crump, G. Erbert, H. Wenzel, C. Frevert, C. M. Schultz, K.-H. Hasler, R. Staske, B. Sumpf, A. Maaßdorf, F. Bugge, S. Knigge, and G. Traenkle, *J. Sel. Top. Quantum Electron.* **19**, 1501211 (2013).

<sup>8</sup>Crosslight Software, Inc., see <http://www.crosslight.com> for software details.

<sup>9</sup>J. Piprek, *Semiconductor Optoelectronic Devices: Introduction to Physics and Simulation* (Academic Press, San Diego, 2003), Chap. 9.

<sup>10</sup>B. Galler, P. Drechsel, R. Monnard, P. Rode, P. Stauss, S. Froehlich, W. Bergbauer, M. Binder, M. Sabathil, B. Hahn, and J. Wagner, *Appl. Phys. Lett.* **101**, 131111 (2012).

<sup>11</sup>B. Galler, Ph.D. thesis, Albert Ludwigs University, Freiburg, Germany, 2014 (in German).

<sup>12</sup>F. Bernardini, in *Nitride Semiconductor Devices: Principles and Simulation*, edited by J. Piprek (Wiley VCH, Weinheim, 2007), Chap. 3.

<sup>13</sup>J. Pal, G. Tse, V. Haxha, and M. A. Migliorato, *Phys. Rev. B* **84**, 085211 (2011).

<sup>14</sup>J. Piprek, F. Roemer, and B. Witzigmann, *Appl. Phys. Lett.* **106**, 101101 (2015).

- <sup>15</sup>A. Pourhashemi, R. M. Farrell, D. A. Cohen, J. S. Speck, S. P. DenBaars, and S. Nakamura, *Appl. Phys. Lett.* **106**, 111105 (2015).
- <sup>16</sup>J. Piprek, *Appl. Phys. Lett.* **107**, 031101 (2015).
- <sup>17</sup>J. Piprek and S. Nakamura, *IEE Proc.: Optoelectron.* **149**, 145 (2002).
- <sup>18</sup>E. Kioupakis, P. Rinke, and C. G. Van de Walle, *Appl. Phys. Express* **3**, 082101 (2010).
- <sup>19</sup>B. P. Yonkee, E. C. Young, C. Lee, J. T. Leonard, S. P. DenBaars, J. S. Speck, and S. Nakamura, *Opt. Express* **24**, 7816 (2016).
- <sup>20</sup>S. Nozaki, S. Yoshida, K. Yamanaka, O. Imafuji, S. Takigawa, T. Katayama, and T. Tanaka, *Jpn. J. Appl. Phys., Part 1* **55**, 04EH05 (2016).